Robust RFID Localization in Multipath with Phase-Based Particle Filtering and a Mobile Robot

Evangelos Giannelos, Emmanouil Andrianakis, Konstantinos Skyvalakis, Antonis G. Dimitriou, *Senior Member, IEEE* and Aggelos Bletsas, *Senior Member, IEEE*

Invited Paper

***Abstract*—This work revisits particle filtering RFID localization methods, solely based on phase measurements. The reader is installed on a low-cost robotic platform, which performs autonomously (and independently from the RFID reader) open source simultaneous localization and mapping (SLAM). In contrast to prior art, the proposed methods introduce a weight metric for each particle-measurement pair, based on geometry arguments, robust to phase measurement noise (e.g., due to multipath). In addition, the methods include the unknown constant phase offset as a parameter to be estimated. No reference tags are employed, no assumption on the tags' topology is assumed and special attention is paid for reduced execution time. It is found that the proposed phase-based localization methods offer robust performance in the presence of multipath, even when the tag phase measurements are variable in number and sporadic. The methods can easily accommodate a variable number of reader antennas. Mean absolute localization error, relevant to the maximum search area dimension, in the order of 2% - 5% for 2D localization and 9.6% for 3D localization was experimentally demonstrated with commodity hardware. Mean absolute 3D localization error in the order of 24 cm for RFID tags in a library was shown, even though the system did not exploit excessive bandwidth or any reference tags. As a collateral dividend, the proposed methods also offer a concrete way to classify the environment as multipath-rich or not.**

I. Introduction

RFID localization has been attracting considerable excitement within the RFID and wireless research community. A growing interest has been observed lately, perhaps due to the following reasons: a) improved tag chip sensitivity and respective reading range and b) availability of channel state information (CSI), including RSSI and phase, from commodity readers. Even though RSSI has been extensively exploited in RF localization research, phase-based techniques have recently appeared in the RFID localization literature [1]–[8].

Phase measurements introduce by definition an ambiguity in distance, measured in wavelength multiples (for one-way wireless communication) or half-wavelength multiples (for roundtrip backscatter communication). Such ambiguity can be mitigated exploiting various wavelengths and increased bandwidth [9] or mobility, i.e., taking measurements at multiple positions, with either the tags or the reader in motion [2], [5]–[8]. Motion of the reader imposes additional challenges, such as reader location estimation [7], further challenging the tag localization problem. Other techniques include angle-of-arrival estimation through mobility of the reader [10] or reference tags at known locations (e.g. [6], [10]). Furthermore, RFID tag localization based on excessive bandwidth [11] has been also proposed. Super-resolution techniques based on tens of megahertz bandwidth and multi-antenna terminals have been also studied in the context of wireless CSI-based WiFi localization [12]. Even though excessive bandwidth assists in impressive localization accuracy, Gen2 RFID operation (e.g., in European UHF ISM bands) is not compatible with tens of megahertz bandwidth. The literature is constantly evolving and the above list, is by no means complete.

An important limitation in phase-based localization techniques is due to wireless multipath. In an effort to mitigate multipath, phase-based localization methods typically require a large number of measurements. This work revisits particle filtering (PF) localization methods, solely based on phase; it is shown that the proposed methods are robust to sporadic and variable number of measurements. The reader is installed on a low-cost robotic platform, which performs autonomously (and independently from the RFID reader measurements) simultaneous localization and mapping (SLAM), with open source algorithms. The goal is to localize commodity, wide-spread, Gen2 RFID tags, without any reference tags, while operating in multipath-rich environments under limited bandwidth. A 2D and a 3D localization scenario examined can be seen in Fig. 4 and Fig. 7, respectively.

Compared to phase-based localization research [3], [6], [7], our particle filtering methods introduce a different distance metric of each particle-measurement phase pair, based on geometry arguments, more robust to phase measurement noise (e.g., due to multipath). In contrast to [7], the methods include the unknown *constant* phase offset as a variable (or a parameter) to be considered and estimated, while no assumption is made on the 3D topology of the tags to be localized. Work in [13] used PF but without phase measurements. No reference tags are used in this work; in addition, no special exploitation of the reader antenna characteristics (e.g., gain and directivity) [14] is made, that could assist in the localization process. In addition, the method directly accommodates variable number of reader antennas and special attention is paid for reduced

Invited from the 15th IEEE International Conference on RFID, April 2021, Atlanta, Georgia. This research has been co-financed by the European Union and Greek national funds through the Operational Program Competitiveness, Entrepreneurship and Innovation, under the call RESEARCH - CREATE - INNOVATE (project code: T1EDK-03032). A. Dimitriou is with Dept. of ECE, Aristotle University of Thessaloniki, Thessaloniki 54453, Greece. The rest of the authors are with School of ECE, Technical Univ. of Crete, Chania, Greece 73100. Email: {egiannelos@isc.tuc.gr, eandrianakis@isc.tuc.gr, kskyvalakis@isc.tuc.gr, antodimi@ece.auth.gr, aggelos@telecom.tuc.gr}

execution time.

Section II offers the system model and Section III presents basic calculations with phase measurements; Section IV describes the phase-based particle filtering method and its variations, highlighting the differences with prior art; Section V offers the experimental results; finally, work is concluded in Section VI.

Notation: $\angle z$ denotes the phase of complex number z, $\mathcal{N}(x, m, \sigma^2)$ stands for the normal distribution with mean m, variance σ^2, evaluated at x, $\mathcal{U}[a, b]$ denotes the uniform distribution in $[a, b]$ and $\mathbb{N}$, $\mathbb{Z}$ denote the set of natural and integer numbers, respectively.

II. System Model

RFID tag location is denoted as $\boldsymbol{x}_{\mathrm{T}} \triangleq [x_{\text{tag}}\ y_{\text{tag}}\ z_{\text{tag}}]^T$ and similarly, reader location as $\boldsymbol{x}_{\mathrm{R}}$. It is further assumed that measured phase at the reader $\phi_{\text{meas}}^{[t]}$ at time t is also accompanied by knowledge of the reader location $\boldsymbol{x}_{\mathrm{R}}^{[t]}$ at that measurement instance. Modeling of $\phi_{\text{meas}}^{[t]}$ follows, with time dependence (temporarily) dropped, for clarity.

RFID reader transmits a signal with carrier frequency f_{c} and phase ϕ_{R}; the received carrier signal at the tag will be received with a time delay of $\tau = d_0/c = d_0/(\lambda f_{\mathrm{c}})$, where $d_0 \triangleq ||\boldsymbol{x}_{\mathrm{R}} - \boldsymbol{x}_{\mathrm{T}}||_2$ is the Euclidean distance between reader and tag antennas, c is the speed of light and λ is the carrier wavelength; this is equivalent to a signal received at the tag with phase as follows:

$$\phi_{\mathrm{R}} - 2\pi f_{\mathrm{c}}\tau = \phi_{\mathrm{R}} - 2\pi d_0/\lambda = \phi_{\mathrm{R}} - k\, d_0,$$

where $k = 2\pi/\lambda$ is the angular wavenumber. Thus, the (one-way) flat-fading wireless channel induces a phase of $-kd_0$, assuming no other propagation paths.

In case of multipath between reader and tag, the (one-way) flat fading channel can be written as follows:

$$h = \underbrace{a_0 e^{-jkd_0}}_{\text{direct path}} + \underbrace{\sum_{i=1}^{\mathsf{N_m}} a_i e^{-jkd_i}}_{\text{multipath}} \tag{1}$$

$$= \underbrace{a_0 e^{-jkd_0}}_{h_0} \underbrace{\left(1 + \sum_{i=1}^{\mathsf{N_m}} \frac{a_i}{a_0} e^{-jk(d_i - d_0)}\right)}_{h_{\mathsf{m}}} \tag{2}$$

$$= h_0\, h_{\mathsf{m}}, \tag{3}$$

where d_i is the length of the i-th propagation path (out of $\mathsf{N_m}$), that depends on the location of the reflectors, as well as the locations of the reader and tag, while complex coefficients $a_i, i \in \{1, \ldots, \mathsf{N_m}\}$ depend on space geometry, reflector's dielectric constants and antenna gains. Thus, the induced phase of the roundtrip (two-way) propagation channel h^2 (i.e., from reader-to-tag and back) can be written as follows:

$$\phi_{\text{prop}} \equiv \angle h^2 = 2\,(\angle h_0 + \angle h_{\mathsf{m}}) = -2kd_0 + 2\angle h_{\mathsf{m}}. \tag{4}$$

The measured phase at the reader is also affected by the tag itself, since the tag's reflection coefficient depends on the terminating load, which in turn, depends on tag's received power; the latter is due to various reasons, including the non-linear rectifier at the RFID tag that harvests energy from the incoming RF signal. Thus, the tag itself induces in the phase measurement a term of ϕ_{tag} [1] that depends on reader's transmit power, reader's location and tag's location (since that term depends on tag's received power). In addition to that, there are additional delays due to cabling (corresponding to constant phase offset $\hat{\phi}_0$), as well as phase noise $\hat{\phi}_n$ at the reader's receive chain:

$$\phi_{\text{out}} = \phi_{\mathrm{R}} + \phi_{\text{prop}} + \hat{\phi}_0 + \phi_{\text{tag}} + \hat{\phi}_n, \tag{5}$$

$$= -2kd_0 + \underbrace{\phi_{\mathrm{R}} + \hat{\phi}_0}_{\theta} + \underbrace{2\angle h_{\mathsf{m}} + \phi_{\text{tag}} + \hat{\phi}_n}_{\phi_n}, \tag{6}$$

$$= -\frac{4\pi d_0}{\lambda} + \theta + \phi_n. \tag{7}$$

Thus, the received phase can be safely modeled by Eq. (7), where the (useful) term $-2k||\boldsymbol{x}_{\mathrm{R}} - \boldsymbol{x}_{\mathrm{T}}||_2$ is perturbed by a constant unknown phase term θ and a variable unknown term ϕ_n. In rich multipath conditions, ϕ_n can vastly change (due to $\angle h_{\mathsf{m}}$), even with location changes of the tag or the reader, in the order of a fraction of one wavelength. Thus,

$$\phi_{\text{out}} \neq \phi_{\text{out}}(d_0), \tag{8}$$

or in other words, end-2-end phase ϕ_{out} does not *only* depend on distance between tag and reader; it also depends on the specific tag and reader utilized, as well as on the environment.

From Eq. (7) it can be seen that any distance d_0 with

$$d_0 = \delta\rho + n\,\lambda/2, n \in \mathbb{N},\ \delta\rho \in [0, \lambda/2), \tag{9}$$

where $\delta\rho$ equals to $d_0 \mod \lambda/2$, outputs the same phase measurement for given value of noise. Thus, phase measurements introduce distance ambiguity that must be explicitly addressed by the localization algorithm.

The reader typically reports a value in $[-\pi, \pi)$ or $[0, 2\pi)$. The reader in the conducted experiments utilize the latter, and thus,

$$\phi_{\text{meas}} = \phi_{\text{out}} \bmod 2\pi, \tag{10}$$

$$\overset{(*)}{=} \left[-\frac{4\pi d_0}{\lambda} \bmod 2\pi + \underbrace{\theta \bmod 2\pi}_{\hat{\phi}} + \underbrace{\phi_n \bmod 2\pi}_{\hat{\phi}_n}\right] \bmod 2\pi,$$

$$= \left[-\frac{4\pi d_0}{\lambda} \bmod 2\pi + \hat{\theta} + \hat{\phi}_n\right] \bmod 2\pi, \tag{11}$$

where in $(*)$, the property $(\alpha + \beta) \bmod \gamma = [(\alpha \bmod \gamma) + (\beta \bmod \gamma)] \bmod \gamma$ was exploited and both $\hat{\theta}, \hat{\phi}_n$ have support in $[0, 2\pi)$.

III. Phase-based Preliminaries

It is common in the literature to find expressions of the measured phase, as in Eq. (7), omitting the minus sign, i.e.,

$$\phi_{\text{out}} = +\frac{4\pi d_0}{\lambda} + \theta + \phi_n. \tag{12}$$

That is also valid, since the sign of the channel-dependent term $\frac{4\pi d_0}{\lambda}$ informs whether phase is added or subtracted to

the phase of the reader, while no assumption has been made on the value of the unknown constant noise term θ in Eq. (7).

However, the transformation from phase measurement ϕ to distance d_0 and vice versa, should explicitly state which formula is used; this is important, since $\phi_- \neq \phi_+$, for phases defined as:

$$\phi_- = -\frac{4\pi d_0}{\lambda} \bmod 2\pi, \tag{13}$$

$$\phi_+ = +\frac{4\pi d_0}{\lambda} \bmod 2\pi. \tag{14}$$

For any $\phi \in [0, 2\pi)$, it can be easily seen that $\delta\rho$ in Eq. (9) is given as follows:

$$\delta\rho = \begin{cases} \frac{\lambda}{2}\left(1 - \frac{\phi}{2\pi}\right), & \text{for } \phi = -\frac{4\pi d_0}{\lambda} \mod 2\pi, \\ \lambda\,\phi/(4\pi), & \text{for } \phi = +\frac{4\pi d_0}{\lambda} \mod 2\pi. \end{cases} \tag{15}$$

Therefore, any phase-based localization algorithm should explicitly state which transformation of the two in Eqs. (13), (12) exploits.

IV. Robust Distance-based Particle Filtering Methods (RDPF)

Assume a given pair $(\phi^{[t]}_{\text{meas}}, \boldsymbol{x}^{[t]}_{\text{R}})$ of phase measurement and respective reader location. Testing whether a particular tag location $\boldsymbol{x}^*_{\text{T}} \triangleq \left[x^*_{\text{tag}}\ y^*_{\text{tag}}\ z^*_{\text{tag}}\right]^T$ is likely to produce such specific phase measurement requires the conditional likelihood pdf $p\left(\cdot|\cdot\right)$ of phase measurement given the specific tag location:

$$w^* = p\left(\phi^{[t]}_{\text{meas}} | \boldsymbol{x}^*_{\text{T}}, \boldsymbol{x}^{[t]}_{\text{R}}\right). \tag{16}$$

Testing various possible samples of tag locations and acquiring the respective weights can, in principle, offer the expected value of the unknown tag location (or the expected value of any function of the unknown location). The basic requirement is that the number of samples (or *particles*) must be *sufficiently* large. Particle filtering is based on the theory of importance sampling and has been extensively used in the robotics community.

An implicit requirement is knowledge of the conditional likelihood pdf. One approach followed in [7] is to convert distance $d = ||\boldsymbol{x}^{[t]}_{\text{R}} - \boldsymbol{x}^*_{\text{T}}||_2$ to phase $\phi^* \in [0, 2\pi)$ using Eq. (13) (or (14)) and utilize distance $\delta\phi = |\phi^* - \phi^{[t]}_{\text{meas}}|$ as a metric, through a Gaussian Kernel [7, page 6]):

$$w^* \propto e^{-\delta\phi^2/(2\sigma^2_\phi)}.$$

Distance metric equal to $\delta\phi = |\phi^* - \phi^{[t]}_{\text{meas}}|$ between measured phase ϕ_{meas} and expected (noiseless) phase ϕ^* for a given tag location, has been also used in [3, Eq. (8)] and [6, Eq. (5)].

This work follows a different approach that explicitly accommodates phase measurement noise (due to multipath or other sources); if $\phi^* = \delta_\epsilon \to 0^+$ and $\phi^{[t]}_{\text{meas}} = 2\pi - \delta_\epsilon \to 2\pi$, then $\delta\phi = 2\pi - 2\delta_\epsilon \to 2\pi$, i.e., the distance metric assumes a large value and correspondingly, the weight will be small. Due to multipath and other noise sources (shown in Eq. (7)), as well as the modulo operation, a small perturbation of an angle close to 0 may change it to a new value close to 2π. Thus, the distance metric between an angle close to 0 and an angle close to 2π should be small and the corresponding weight should be large. The following approach accommodates the above and utilizes distances instead of phases to find out the appropriate weight metric.

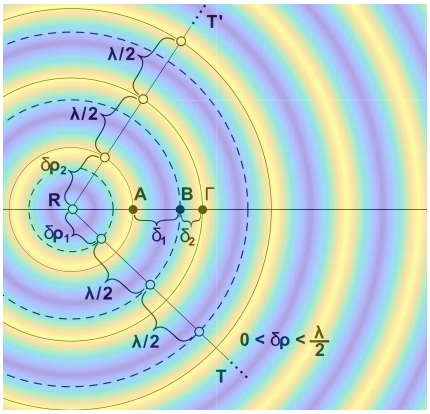

Fig. 1: Visualization of the smallest distance Δ between a given sample point in space (**B**) for a given RFID phase measurement, converted to distance. The color shade depicts the weight values according to Eq. (25). Reader is located at point R.

Specifically, using Eq. (15) and Eq. (9) the measured phase $\phi^{[t]}_{\text{meas}}$ is converted to distance. The latter defines in 2D (3D), the concentric circles (spheres), centered at the corresponding robot location, where the tag is located (based on the measurement). The closest distance between these circles (spheres) and $\boldsymbol{x}^*_{\text{T}}$ defines the utilized metric Δ of this work.

Fig. 1 assists in visualizing the above; $d = ||\boldsymbol{x}^{[t]}_{\text{R}} - \boldsymbol{x}^*_{\text{T}}||_2$ is converted to the expression of Eq. (9), with $\delta\rho = d \mod \lambda/2$. Thus, for each sample and given phase measurement there are totally two distance equations of the following form:

$$\delta_1 = \delta\rho_1 + n_1(\lambda/2),\ n_1 \in \mathbb{N}, \tag{17}$$

$$\delta_2 = \delta\rho_2 + n_2(\lambda/2),\ n_2 \in \mathbb{N},\ \delta\rho_1 > \delta\rho_2, \tag{18}$$

with both $\delta\rho_1, \delta\rho_2 \in [0, \lambda/2)$. Which of the two equations above correspond to phase measurement or particle distance is not needed; d_1 simply corresponds to the equation with the largest $\delta\rho$. With the help of Fig. 1 and simple calculations, it is easy to see that the minimum distance Δ described above is given by:

$$\Delta = \min(\delta_1, \delta_2) = \min\left(\delta\rho_1 - \delta\rho_2, \frac{\lambda}{2} - (\delta\rho_1 - \delta\rho_2)\right). \tag{19}$$

Notice that the case of a pair of phases described above, where one is close to 0 (rad) and another close to 2π (rad) corresponds to a pair of $\delta\rho_1, \delta\rho_2$ where the first is close to $\lambda/2$ (m) and the second is close to 0 (m). The above formula will offer a small distance metric Δ.

In addition, this work explicitly takes into account the constant offset θ. Prior work in [7] did not include it in the particle filter parameters, since specific tag topologies were tested (i.e., tags at the same height). This work will not assume

specific RFID topologies. Assuming a sample value θ^*, the following steps are needed:

$$\phi^* = \left(\phi^{[t]}_{\text{meas}} - \theta^*\right) \bmod 2\pi, \tag{20}$$

$$\delta\rho_\phi = \begin{cases} \frac{\lambda}{2}\left(1 - \frac{\phi^*}{2\pi}\right), & \text{if } \phi_{\text{out}} = -\frac{4\pi d_0}{\lambda} + \theta + \phi_n, \\ \lambda\,\phi^*/(4\pi), & \text{if } \phi_{\text{out}} = +\frac{4\pi d_0}{\lambda} + \theta + \phi_n, \end{cases} \tag{21}$$

$$\delta\rho_d = ||\boldsymbol{x}^{[t]}_{\text{R}} - \boldsymbol{x}^*_{\text{T}}||_2 \bmod \lambda/2, \tag{22}$$

$$\delta\rho_1 = \max(\delta\rho_\phi, \delta\rho_d), \tag{23}$$

$$\delta\rho_2 = \min(\delta\rho_\phi, \delta\rho_d), \tag{24}$$

and $\delta\rho_1, \delta\rho_2$ are used as input to Eq. (19). Notice that expression in Eq. (21) above changes according to which phase vs distance transformation is adopted, i.e., Eq. (13) or (14).

With this metric Δ, weight particle is given as follows:

$$w^* \propto e^{-\Delta^2/(2\sigma^2)}, \tag{25}$$

where σ has units of distance and σ^2 depends on the power of the phase measurement noise, including all sources (e.g. multipath). In strong multipath environments and measurements spanning a large area (e.g., using a moving robot), this value should be increased. It was experimentally found that in low multipath conditions, values of σ around 0.1λ worked best, while in strong multipath, values around of λ were more suitable. In the numerical experiments below, the value of σ was 0.1λ and λ in campaign 1 and campaigns 2-4, respectively. An agnostic approach to classify the environment will be described later, when RDPF2 is introduced.

For multiple measurements available for a given tag, the measurements are assumed independent and for a given sample, there are as many weights as the number of measurements; thus, for each sample (particle), the overall weight is the product of the weights. Variations of the algorithm can include resampling of the weights, e.g., using the low-variance resampler [15], with or without replacement of the particles. Given that the RFID tags (target to be located) in the experiments are static, we omitted the resampling step; improvements due to resampling are smaller in static than in mobile target localization [15].

The algorithm is summarized as RDPF1 below; initialization of the particles assumes a uniform distribution per dimension and requires boundaries of the search area space; the latter is $4-$dimensional for 3D localization and $3-$dimensional for 2D localization, due to the existence of offset θ. Other initialization distributions are possible. In order to utilize the algorithm's capacity to accommodate multiple antennas, we just need to provide the measurement pairs (line 11) as $\left\{\phi^{[t]}_{\text{meas}}, \boldsymbol{x}^{[t]}_{\text{A}}\right\}$, where $\boldsymbol{x}^{[t]}_{\text{A}}$ is the reader antenna's location, treating measurements of different antennas simply as unique measurements. The algorithm runs independently N times[1] for the same measurement data to extract statistical data. In the general case only one repetition is needed for RDPF1.

[1]100 times in campaigns 1-3 and 10 in campaign 4, in numerical results.

RDPF Algorithm: RDPF1

1: **Initialization of Variables:**
2: Set M (number of Particles), N (number of Epochs)
3: Set $X^a_{\text{min}}, X^a_{\text{max}}, Y^a_{\text{min}}, Y^a_{\text{max}}, Z^a_{\text{min}}, Z^a_{\text{max}}, \theta_{\text{min}}, \theta_{\text{max}}$ (search area dimensions)
4: Set T (time window of collected phase measurements)
5: **for** $n = 1 : N$ **do**
6: **Initialization of All Particles:** $\forall\ m = 1 : M$
7: $x^{[m]} \sim \mathcal{U}[X^a_{\text{min}}, X^a_{\text{max}}]$, $y^{[m]} \sim \mathcal{U}[Y^a_{\text{min}}, Y^a_{\text{max}}]$,
8: $z^{[m]} \sim \mathcal{U}[Z^a_{\text{min}}, Z^a_{\text{max}}]$
9: $\theta^{[m]} \sim \mathcal{U}[\theta^a_{\text{min}}, \theta^a_{\text{max}}]$
10: $\boldsymbol{\chi}^{[m]} = \left[x^{[m]}\ y^{[m]}\ z^{[m]}\ \theta^{[m]}\right]^T$
11: **Select** T measurement pairs $\left\{\phi^{[t]}_{\text{meas}}, \boldsymbol{x}^{[t]}_{\text{R}}\right\}$
12: Initialize all particle weights: $w^{[m]} = 1, \forall\, m = 1 : M$
13: **for** t = 1 : T **do** { measurement index}
14: **for** m = 1 : M **do** { particle index }
15: Set $\boldsymbol{x}^*_{\text{T}} = \left[x^{[m]}\ y^{[m]}\ z^{[m]}\right]^T$ from $\boldsymbol{\chi}^{[m]}$
16: Set $\theta^* = \theta^{[m]}$ from $\boldsymbol{\chi}^{[m]}$
17: Calculate $\delta\rho_1, \delta\rho_2$ (in m) from Eqs. (20)-(24)
18: Calculate Δ (in m) from Eq. (19)
19: $w^{[m]} = w^{[m]}\, p\left(\Delta|\boldsymbol{\chi}^{[m]}\right) \equiv w^{[m]}\, \mathcal{N}\left(\Delta; 0, \sigma^2\right)$
20: **end for**
21: Weight Normalization:
22: $w^{[m]} = w^{[m]} / \sum_{m=1}^{M} w^{[m]}$, $\forall\, m = 1 : M$
23: % Optional: Low Variance Particle Resampling
24: **end for**
25: $\hat{\boldsymbol{x}}^{[n]}_{\text{T}} = \sum_{m=1}^{M} w^{[m]}\, \boldsymbol{\chi}^{[m]} = \left[\hat{x}^{[n]}_{\text{tag}}\ \hat{y}^{[n]}_{\text{tag}}\ \hat{z}^{[n]}_{\text{tag}}\ \hat{\theta}^{[n]}\right]^T$
26: **end for**

A. Modifications for Accelerated Execution: RDPF2

In an effort to keep offset θ as an unknown, while reducing the execution time, the above algorithm is modified. Each sample contains only the tag coordinates and not θ, while the external loop (line 5) tests a specific θ, *common for all particles*. In that way, the same number of particles M corresponds to a smaller search space or equivalently, a smaller number of particles can be exploited.

In this second version, coined as RDPF2, line 9 is omitted and initialization is modified to search θ with resolution $\delta\theta = (\theta_{\text{max}} - \theta_{\text{min}})/N$ (N was set to 100 for observations while lower numbers also perform similarly). The set of measurements is used again over every tested value of θ and the algorithm reports the mean of the tag's location across all tested values of θ. The following lines of RDPF1 are modified:

10: $\boldsymbol{\chi}^{[m]} = \left[x^{[m]}\ y^{[m]}\ z^{[m]}\right]^T$
16: Set $\theta^* = \theta_{\text{min}} + (n-1)\,\delta\theta$
25: $\hat{\boldsymbol{x}}^{[n]}_{\text{T}} = \sum_{m=1}^{M} w^{[m]}\, \boldsymbol{\chi}^{[m]} = \left[\hat{x}^{[n]}_{\text{tag}}\ \hat{y}^{[n]}_{\text{tag}}\ \hat{z}^{[n]}_{\text{tag}}\right]^T$

and line 27 was added to report final location estimate:

27: $\hat{\boldsymbol{x}}_{\text{T}} = \frac{1}{N}\sum_{n=1}^{N} \hat{\boldsymbol{x}}^{[n]}_{\text{T}} = [\hat{x}_{\text{tag}}\ \hat{y}_{\text{tag}}\ \hat{z}_{\text{tag}}]^T$

Experimental results show that RDPF2 can run one order of magnitude faster than RDPF1, while retaining comparable performance. Moreover, it was found experimentally that the tag

location estimate varies almost continuously, across different values of θ in light multipath, as opposed to rich multipath environments. Thus, RDPF2 could be further examined as a potential classifier of the environment, in terms of multipath richness. Additionally, a single random θ value could be chosen and this method could produce satisfactory results in a fraction of the time.

V. Performance Evaluation

Four indoor experimental campaigns were conducted, with an Impinj Speedway R420 RFID reader. Using Impinj's LTK API, a software was developed to control the reader's parameters. One MTI MT-242032 7 dBic reader antenna and up to three FlexiRay SF-2110 5 dBi antennas were utilized. Reader transmission (Tx) power was configured in the range of 20 dBm to 30 dBm.[2] In all campaigns, increasing the reader Tx power also increased the number of tag measurements. In the first campaign (Fig. 2) the tag was successfully interrogated at 56 and 20 positions, at Tx power of 30 and 20 dBm, respectively. For the second and third (Fig. 4) campaigns, each tag was interrogated approximately 900 times at 30 dBm and about 400 times at 20 dBm. For the fourth and last campaign, each tag was interrogated about 300 times (4 tags could not be interrogated) and about 100 times (51 tags could not be interrogated) at 30 and 20 dBm, respectively. Due to the low percentage of unique tags being successfully interrogated, the 20 dBm measurements were not used in this campaign. For comparison purposes, two state-of-the-art phase-based methods were also implemented: BackPos [4] and Relock [8]. Mean absolute localization error (MAE) $\mathrm{E}[|\mathbf{e}|]$ and root mean squared localization error (RMSE) $\sqrt{\mathrm{E}[|\mathbf{e}|^2]}$ will be utilized, with $\mathbf{e} \triangleq ||\hat{\boldsymbol{x}}_\mathrm{T} - \boldsymbol{x}_\mathrm{T}||_2$.

A. Light-multipath (Campaign 1)

In the first campaign (Fig. 2), a single MTI MT-242032 antenna was connected to the reader via a 0.9 dB loss coaxial cable and an Alien ALN-9540 (Higgs-2) tag was placed at a fixed location in an open-space indoor environment. The antenna was moved manually along a 3 m line at intervals of 5 cm, while the tag was placed at the bisector of the antenna's trajectory at a distance of 1 m. The antenna and the tag were placed at a height of 1.52 m. At every position of the antenna, tag interrogations were conducted for 4 secs per Tx power level.

Following the acquisition of the measurements, for every position and power level, a modified mean of the phase was calculated. This modification was necessary due to the noise induced on the measurements by the environment and the electrical components of the equipment. For example, at distance that should correspond to a phase measurement close to 360° (or 0°), even a small noise perturbation can push some measurements over 360° (or below 0°) resulting in some measurements appearing in the 0° (or 360°) region because of phase wrapping. Thus, a classic mean approach would result in a value shifted to the center of the phase spectrum, failing to produce a useful value. Instead, when such cases are detected the following approach is utilized: the phase range is divided in two regions, 0-180° and 180-360°. The measurements of the least populated region are wrapped around (e.g. values in 0-10° would be mapped to 360-370°) and then the mean is calculated applying a modulo operator if needed.

[2]Cable losses as well as reader's output power were measured using a VNA and a spectrum analyzer, respectively.

Fig. 2: Baseline experimental campaign 1: light multipath environment with manual movement of the reader antenna.

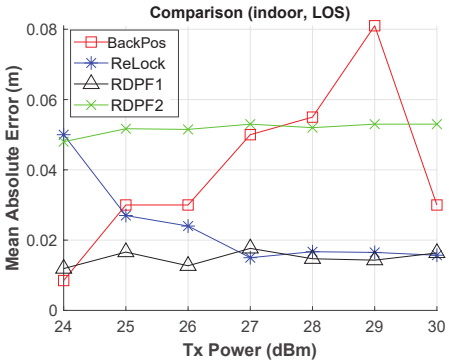

Fig. 3: Campaign 1 localization error vs Tx power.

Results for this campaign are depicted in Fig. 3. All methods performed satisfactorily in terms of MAE, with satisfying results below 2 cm for higher Tx power (as shown in Fig. 3). Such absolute error corresponds to less than 2% of the tag-to-reader range, set at 1 m in the first campaign. However we noticed that ReLock's performance is improving with the number of measurements, while RDPF1 and RDPF2 do not seem to be affected. BackPos was also found to be sensitive on the number of available measurements, while the increase of error with larger Tx power is probably due to stronger multipath when Tx power is increased.

For the RDPF methods, the search area used for the initialization of the particles was set to 1 m × 1 m. The number of particles was set to $M = 10^5$ for RDPF1 and $M = 10^4$ for RDPF2, since the latter does not randomize the θ in each particle, but instead uses a common θ for all particles and thus, needs less particles to populate the search space adequately. Notice that due to the same height of tags and reader antenna, the tag localization problem has two unknowns $x_\mathrm{tag}, y_\mathrm{tag}$, in order to compare with BackPos, which is a 2D tag localization method by construction. Execution times were all under 1 sec,

due to the relatively low number of measurement locations.

B. Rich-multipath (Campaigns 2-3)

In the second campaign, the manual reader movement setup of campaign 1 was utilized, but in a multipath richer environment, with two variations: A) 15 tags on books, packed on a bookshelf, with an average distance of 5.5 cm, and B) only the two books at the opposing ends of the bookshelf are equipped with a tag, as shown in the right part of Fig. 4. Reader, antenna and cables were the same as before. Measurements were taken every 5 cm, the same way as in the first campaign. The purpose of this campaign was to test the algorithms, without worrying about the robot-reader (used in the next campaigns) self-localization error, while inducing additional reflections and multipath among tags; additionally, the close proximity among tags in case A pushed their operational limits, due to coupling. In this campaign, Alien ALN-9740 (Higgs-4) tags were used. The results for case A are depicted in Table I. The presence of multiple tags, next to each other, did not seem to produce significant deviations in the performance of the algorithms, so the results for case B are omitted. BackPos offered excessive errors in some cases, probably due to stronger multipath and was subsequently omitted from the following campaigns.

In the third campaign (Fig. 4), a custom robotic setup was utilized with Tx power at 20 and 30 dBm: the robot was a Turtlebot2 with a Kobuki mobile base for motion support, equipped with a Hokuyo UST-20LX LIDAR sensor for SLAM operations and the aforementioned reader. The cable and antenna were replaced by smaller counterparts, a 0.74 dB loss coaxial cable and a FlexiRay SF-2110 5 dBi antenna. The antenna and the tags were placed at a lower height of 1.1m further increasing the contribution of multipath. For more accurate position estimation of the robot, the map of the environment was first created using Google's Cartographer [16] and then during the experiments robot localization was performed using AMCL [17]. The robot's speed was 10 cm/sec; measurements were taken continuously and their distance on average was 0.5 cm. Again, Alien ALN-9740 (Higgs-4) tags were used in this campaign. Results are shown in Table I and Fig. 5.

In both second and third campaigns, RDPF1 and RDPF2 offered similar results and in general outperformed ReLock and BackPos at the lower transmission power of 20 dBm. Since Tx power controlled the number of measurements, it can be safely concluded that RDPF1 and RDPF2 offer robust estimates when number of measurements is variable. Table I offers $\mathbf{e}$, as well as $\mathbf{e}_x \triangleq |\hat{x}_{\text{tag}} - x_{\text{tag}}|$ (i.e., error across the x-axis, which is parallel to the bookshelf), for three tags. Minimum error value per scenario (i.e., campaign and Tx power) among the compared methods is presented in bold.

For the RDPF methods, the search area and particle numbers were the same as before. RDPF1 execution time per repetition per RFID tag for the worst case (i.e., largest number of measurements) was 2.5 sec, while RDPF2 required 0.25 sec per value of θ per tag. For ReLock we implemented a pre-filtering algorithm that finds the maximum window of consecutive measurements so that every location of measurement is within

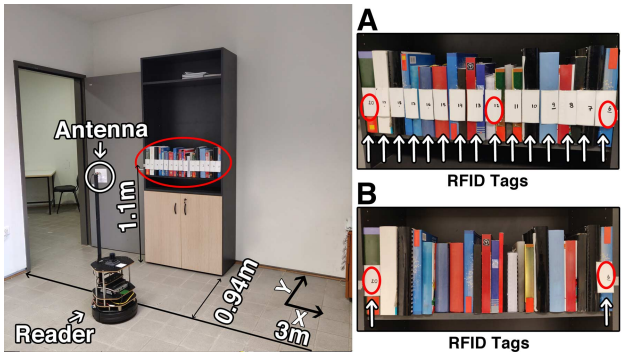

Fig. 4: Campaigns 2-3: indoor harsh multipath environment a commercial RFID reader on an autonomous robotic platform scans and localizes the tags.

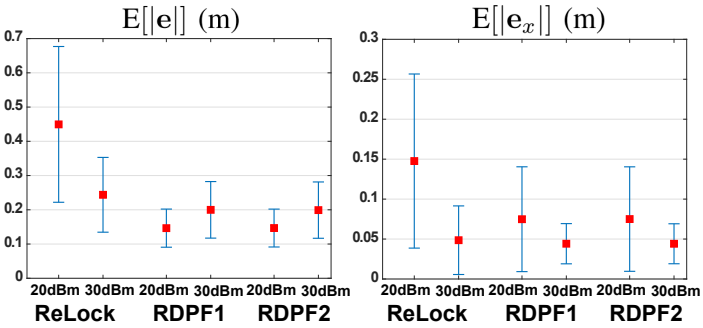

Fig. 5: Campaign 3 (moving robot) average absolute error between 2 standard deviations across all 15 bookshelf tags.

5 cm of the next one. That is because ReLock requires that the phase between two consecutive measurement locations does not change drastically, so that phase unwrapping can function reliably. ReLock execution time per tag at the same processing unit for the largest number of measurements was 0.25 seconds. Taking in mind that the robot moves at rate of 10 cm/sec, a 3-meter trajectory required 30 sec; thus, for the considered scenarios, all the above methods can be considered as "real-time".

Fig. 5 presents the third campaign's average value of $\mathbf{e}$ and $\mathbf{e}_x$ (rectangles) across all 15 tags, within two standard deviations (the vertical lines span 2 standard deviations); at 30 dBm it was observed that the methods perform adequately with error $\mathbf{e}_x$ below 5 cm, which corresponds to relative (to tag-reader distance) error below 5%; however, the RDPF methods presented smaller variance, with standard deviation in the order of 2 cm at 30 dBm Tx power; for the case of 20 dBm Tx power, RDPF1 and RDPF2 outperform Relock, probably due to sensitivity of the latter to the available number of measurements. In terms of average $\mathbf{e}$, RDPF1 and RDPF2 demonstrated approximately 15 cm (corresponding to 15% relative to distance error) with standard deviation of 5 cm at 20 dBm, where Relock showed increased error, due to smaller number of measurements. Interestingly, $\mathbf{e}$ for RDPF1, RDPF2 was smaller in 20 dBm than in 30 dBm.

Finally, Fig. 6 depicts estimated $\hat{y}_{\text{tag}}$ of RDPF2 as a function of θ, for first campaign (LOS/light multipath) and third campaign (strong multipath). It can be seen that $\hat{y}_{\text{tag}}$ varies

TABLE I: Experimental results of the bookshelf campaigns with all 15 tags placed (case A).

			Tag ID					
			#20 leftmost tag		#12 center tag		#6 rightmost tag	
			E[|**e**|] (m)	E[|$\mathbf{e}_x$|] (m)	E[|**e**|] (m)	E[|$\mathbf{e}_x$|] (m)	E[|**e**|] (m)	E[|$\mathbf{e}_x$|] (m)
Campaign 2 - Manual	ReLock	20dBm	0.225	0.033	0.755	0.104	0.112	0.013
		30dBm	**0.016**	**0.012**	**0.032**	0.025	0.048	**0.012**
	RDPF1	20dBm	**0.063**	**0.006**	**0.102**	0.036	**0.029**	0.013
		30dBm	0.103	**0.012**	0.087	**0.017**	**0.018**	0.014
	RDPF2	20dBm	0.067	**0.006**	0.109	0.036	0.050	0.013
		30dBm	0.106	**0.012**	0.079	**0.018**	0.051	0.013
	BackPos	20dBm	0.223	0.043	0.361	0.041	0.194	**0.001**
		30dBm	0.186	0.165	0.091	0.075	0.294	0.293
Campaign 3 - Robot	ReLock	20dBm	0.630	0.211	0.411	0.066	0.621	0.197
		30dBm	0.363	0.090	0.172	**0.036**	0.251	0.058
	RDPF1	20dBm	0.182	**0.099**	**0.132**	**0.021**	0.104	**0.008**
		30dBm	0.254	0.068	**0.158**	0.046	0.138	**0.051**
	RDPF2	20dBm	**0.181**	**0.099**	**0.132**	**0.021**	**0.102**	0.009
		30dBm	**0.251**	**0.067**	**0.158**	0.046	**0.137**	**0.051**

smoothly in light multipath environments (campaign 1), as opposed to strong multipath (campaign 3). This observation can be further exploited for classification purposes of the environment, as multipath-rich or not. For a multipath-poor environment, methods like BackPos will be very useful. Moreover, the same plot implies that θ plays a more important role in light multipath, as opposed to rich multipath environments. These topics will be further examined in future work.

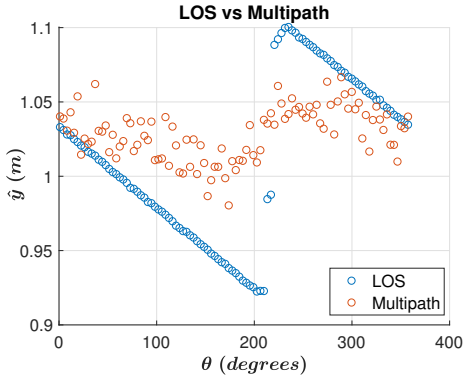

Fig. 6: Visualization of $\hat{y}_{\text{tag}}$ with respect to θ for two different environments: LOS/light multipath (campaign 1) vs strong multipath (campaign 3). This behavior could be exploited for classification of the environment as multipath-rich or not.

C. Rich-multipath - 3D Results (Campaign 4)

In the fourth and final campaign, the robotic setup was utilized once more in a different, multipath-rich environment in order to test the algorithms on multiple environments as well as their performance in 3D localization. There were 70 tags, placed on the backs or the insides of books, having different orientations with respect to the movement of the robot-antennas. The books were atop of metallic shelves, which further increases reflections, at different heights ranging from 0.15 to 2.3 m. The topology can be seen at Fig. 7 and the actual trajectory of the robot, as computed by Cartographer, is shown in Fig. 8.

Regarding the robotic platform, a longer pole was attached so it could accommodate more antennas at larger heights. The number of FlexiRay SF-2110 antennas increased to 3, at heights 1.06, 1.46 and 1.86 m, increasing the area in which tags can be successfully interrogated and resolving localization ambiguity in the vertical ***z-axis***. The search space for this campaign was increased to a 2.5 m $\times$ 1 m $\times$ 2.5 m space while the particle number remained at 10^5. To the best of our knowledge, ReLock does not simultaneously utilize multiple antennas, so it was omitted from this campaign. As it can be seen from the results in Table II, RDPF1 can reliably locate the tags in a 3D space, while having a performance boost with the increase of the number of available measurements. Especially for the cases where the number of measurements is over 200 (average number of measurements is 300), our method can locate the tags with a MAE of 24 cm; the latter corresponds

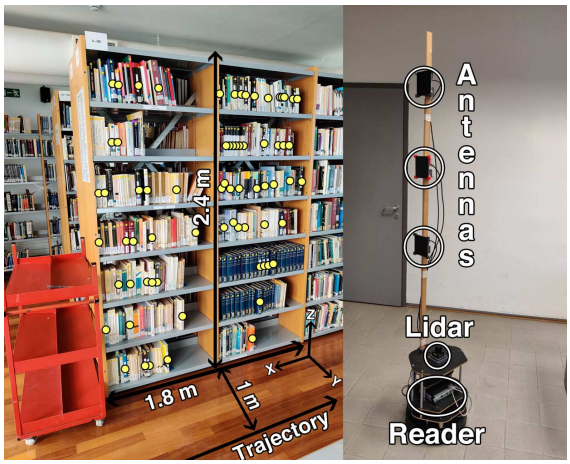

Fig. 7: Campaign 4: topology of RFID tags, trajectory (left) and robotic reader setup (right).

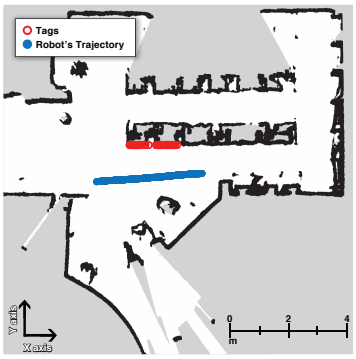

Fig. 8: Campaign 4: Real map of the library produced by the Cartographer algorithm, including robot's estimated trajectory.

to 9.6% of the maximum search space dimension (i.e., 2.5 m in this example). The worst execution time of RDPF1 for the 3D case was 5 sec due to increased number of measurements.

TABLE II: 3D Experimental Results Across 70 Tags.

	$\mathrm{E}[\lvert\mathbf{e}\rvert]$ (m)	$\sqrt{\mathrm{E}[\lvert\mathbf{e}\rvert^2]}$ (m)
Measurements per tag > 50	0.31	0.38
Measurements per tag > 100	0.29	0.36
Measurements per tag > 200	**0.24**	**0.26**

VI. Conclusion

The proposed phase-based localization method offered robust performance in the presence of multipath, even when the tag phase measurements are variable in number and sporadic. The method can easily accommodate a variable number of reader antennas and exploits reader mobility, as well as autonomous robot-reader self-localization. Decimeter-level localization error for RFID tags in a library was shown, even though the system did not exploit excessive bandwidth or any reference tags. A classification method was also found that could assist in characterising the environment as multipath-rich or not. Special attention was also given in order to accelerate algorithm execution for real-time operation, matched with the speed of the robot. Future work will further examine ways that exploit robotics in multipath mitigation.

References

[1] P. V. Nikitin, R. Martinez, S. Ramamurthy, H. Leland, G. Spiess, and K. V. S. Rao, "Phase based spatial identification of UHF RFID tags," in *Proc. IEEE Int. Conf. on RFID*, Orlando, USA, Apr. 2010, pp. 102–109.

[2] R. Miesen, F. Kirsch, and M. Vossiek, "Holographic localization of passive UHF RFID transponders," in *Proc. IEEE Int. Conf. on RFID*, Orlando, USA, Apr. 2011, pp. 32–37.

[3] E. DiGiampaolo and F. Martinelli, "Mobile robot localization using the phase of passive uhf rfid signals," *IEEE Trans. Ind. Electron.*, vol. 61, no. 1, pp. 365–376, Jan. 2014.

[4] T. Liu, L. Yang, Q. Lin, Y. Guo, and Y. Liu, "Anchor-free backscatter positioning for RFID tags with high accuracy," in *Proc. IEEE Int. Conf. on Computer Communications (Infocom)*, Toronto, Canada, Apr. 2014, pp. 379–387.

[5] A. Buffi, P. Nepa, and F. Lombardini, "A phase-based technique for localization of UHF-RFID tags moving on a conveyor belt: Performance analysis and test-case measurements," *IEEE Sensors J.*, vol. 15, no. 1, pp. 387–396, Jan. 2015.

[6] E. DiGiampaolo and F. Martinelli, "A robotic system for localization of passive UHF-RFID tagged objects on shelves," *IEEE Sensors J.*, vol. 18, no. 20, pp. 8558–8568, Oct. 2018.

[7] F. Martinelli, "Simultaneous localization and mapping using the phase of passive UHF-RFID signals," *Journal of Intelligent & Robotic Systems (JINT)*, vol. 94, no. 3-4, pp. 711–725, Jul. 2019.

[8] A. Tzitzis, S. Megalou, S. Siachalou, T. Yioultsis, A. Kehagias, E. Tsardoulias, A. Filotheou, A. Symeonidis, L. Petrou, and A. G. Dimitriou, "Phase ReLock - Localization of RFID tags by a moving robot," in *Proc. IEEE European Conf. on Antennas and Propagation (EuCAP)*, Krakow, Poland, Mar. 2019, pp. 1–5.

[9] D. Vasicht, S. Kumar, and D. Katabi, "Decimeter-level localization with a single WiFi access point," in *Proc. USENIX Symposium on Networked Systems Design and Implementation (NSDI)*, Santa Clara, USA, Mar. 2016, pp. 165–178.

[10] J. Wang and D. Katabi, "Dude, where's my card? RFID positioning that works with multipath and non-line of sight," in *Proc. ACM SIGCOMM*, Hong Kong, China, Aug. 2013, pp. 51–62.

[11] Y. Ma, N. Selby, and F. Adib, "Minding the billions: Ultra-wideband localization for deployed RFID tags," in *Proc. ACM Int. Conf. on Mobile Computing and Networking (Mobicom)*, Snowbird, USA, Oct. 2017, pp. 248–260.

[12] M. Kotaru, K. Joshi, D. Bharadia, and S. Katti, "SpotFi: Decimeter level localization using WiFi," in *Proc. ACM SIGCOMM*, London, United Kingdom, Aug. 2015, pp. 269–282.

[13] V. Sović, A. Athalye, M. Bolić, and P. M. Djurić, "Particle filtering for indoor RFID tag tracking," in *Proc. IEEE Statistical Signal Process. Workshop (SSP)*, Nice, France, Jun. 2011, pp. 193–196.

[14] I. Markakis, T. Samaras, A. C. Polycarpou, and J. N. Sahalos, "An RFID-enabled library management system using low-SAR smart bookshelves," in *Proc. Int. Conf. on Electromagnetics in Advanced Applications (ICEAA)*, Torino, Italy, Sep. 2013, pp. 227–230.

[15] S. Thrun, W. Burgard, and D. Fox, *Probabilistic Robotics*. Cambridge, MA: The MIT Press, 2006.

[16] W. Hess, D. Kohler, H. Rapp, and D. Andor, "Real-time loop closure in 2D LIDAR SLAM," in *Proc. IEEE Int. Conf. on Robotics and Automation (ICRA)*, Stockholm, Sweden, May 2016, pp. 1271–1278.

[17] D. Fox, "KLD-sampling: Adaptive particle filters," in *Proc. Int. Conf. on Neural Information Processing Systems: Natural and Synthetic (NIPS)*, Vancouver, Canada, Oct. 2001, pp. 713–720.

Evangelos Giannelos received the 5-year Diploma degree in Electrical and Computer Engineering from the Technical University of Crete (TUC), Greece, in 2018, where he is currently pursuing his Ph.D. degree. His research interests include methods for low power wireless communications, RFID tag localization, robotics, software and systems development.

Emmanouil Andrianakis received the 5-year Diploma degree in Electrical and Computer Engineering from the Technical University of Crete, Greece, in 2020, where he is currently pursuing his MSc degree. His research interests include RFID tag localization, wireless sensor networks and robotics.

Konstantinos Skyvalakis received the 5-year Diploma degree in Electrical and Computer Engineering from the Technical University of Crete, Greece, in 2018, where he is currently pursuing his MSc degree. His research interests include methods for low power wireless communications, signal processing for backscatter communication, satellite communications.

Antonis G. Dimitriou (S01-M06-SM14) received the diploma and the Ph.D. degree in Electrical and Computer Engineering from the Aristotle University of Thessaloniki, Greece, in 2001, and 2006 respectively. Since 2007, he is with the School of Electrical and Computer Engineering of AUTh, where he currently serves as a teaching and research faculty member. He has participated in more than 20 research projects, 8 of which since 2007 as a principal investigator in the fields of Robotics, RFIDs, and Wireless Sensor Networks. He is currently the coordinator of project "RELIEF", involving continuous RFID inventorying through robotics and project "CULTUREID", where RFID equipment will be installed inside the Archaeological Museum of Thessaloniki to monitor RFID tagged exhibits and track visitors. He was a Management Committee Member in the ICT COST Action IC301 "Wireless Power Transmission for Sustainable Electronics (WiPE)". He is the author or co-author of more than 60 journal and conference papers. Dr. Dimitriou was the recipient of the Ericsson Award of Excellence in Telecommunications in 2001 and co-recipient of the student-paper award in the 2011 IEEE RFID-TA conference. He received the "IEEE Wireless Communications Letters Exemplary Reviewer" award in 2012 and 2014. He is a Senior IEEE Member since February 2014. He also serves as a reviewer for major journals and as a TPC member for international conferences.

Aggelos Bletsas received the Diploma degree (with honors) in Electrical and Computer Engineering from Aristotle University of Thessaloniki, Greece in 1998, and the M.Sc. and Ph.D. degrees from MIT, Cambridge, MA, USA, in 2001 and 2005, respectively. He has worked at Mitsubishi Electric Research Laboratories (MERL), Cambridge, MA and RadioCommunications Laboratory (RCL), Department of Physics, Aristotle University of Thessaloniki. He currently serves as full Professor, School of Electrical & Computer Engineering, Technical University of Crete, Greece. His research interests span the broad area of scalable wireless communications and sensor networking, with emphasis on ultra-low power/cost environmental sensing, backscatter radio and ambiently-powered inference networks. His current focus and contributions are relevant to wireless, batteryless, backscatter sensors for precision agriculture that cost a few Euros, consume a few microWatts and can be read with commodity receivers and smartphones. He has served as Associate Editor of *IEEE Transactions on Wireless Communications* (2015-2021) and *IEEE Wireless Communications Letters* (from foundation in 2011-2016) and Technical Program Committee (TPC) member of major IEEE conferences. Dr. Bletsas was co-recipient of the *IEEE Communications Society 2008 Marconi Prize Paper Award in Wireless Communications*, and various Best Student Paper Awards e.g., in IEEE RFID-TA 2011, IEEE ICASSP 2015, IEEE RFID-TA 2017, MOCAST 2018. He has been included in the Highly-Cited Greek Scientists list. One of his papers is ranked 1st in Google Scholar *Classic Papers in Computer Networks & Wireless Communication*.